High-Frequency Vibration Reduction for Unmanned Ground Vehicles on Unstructured Terrain

Hamza El-Kebir[1⋆], Taha Shafa[1,2⋆], Amartya Purushottam[2,3], Melkior Ornik[1], and Ahmet Soylemezoglu[2]

[1] Department of Aerospace Engineering, University of Illinois Urbana-Champaign, Urbana, IL
[2] Construction Engineering Research Lab, US Army Corps of Engineers, Champaign, IL
[3] Department of Electrical and Computer Engineering, University of Illinois Urbana-Champaign, Urbana, IL

Abstract. High-frequency vibrations encountered during land transit of sensitive payloads have long been known to be a possible cause of payload damage and subsequent mission failure. As sensors are also adversely affected by this phenomenon, we aim to provide a solution to minimize high-frequency noise vibrations without reliance on high performance sensing. Naturally, this presents the need for on-board adaptive control capabilities to reduce sensor noise and damage to secured payloads. Thus, we present a novel approach to reducing high-frequency vibration content (HVC) encountered during transit, with the explicit goal of maintaining a desired vehicle speed while keeping high-frequency vibrations below a given threshold regardless of the terrain characteristics. To this end, we present a two-stage solution consisting of a vibration-compensating speed controller and an optimal tracking controller for control command determination. The proposed controller is implemented on a Clearpath Jackal unmanned ground vehicle and subjected to a priori unknown mixed terrain types. Experiments performed on these varying terrains show that the proposed control architecture is able to adjust the desired robot trajectory to remain below the vibration thresholds defined by the mission objective.

Keywords: Adaptive trajectory planning · Navigation on unstructured terrain · Vibration mitigation

1 Introduction

Adverse effects from high-frequency vibrations can adversely affect critical mission tasks beyond the introduction of sensor noise [7, 9]. These vibrations can cause damage to secured payloads [10, 22] and aggravate the conditions of injured personnel during medical evacuations [3, 21]. These issues naturally give rise to the problem of vibration suppression.

⋆ These authors contributed equally to this work.

In this work, we present a novel approach to reducing the high-frequency vibration content encountered during transit with the explicit goal of maintaining a desired vehicle speed, while keeping high-frequency vibrations below a given threshold regardless of the current terrain type. Our theoretical work and presented implementation are motivated by programs like the Squad Multipurpose Equipment Transport (SMET) program, a US Army program providing a robotic "mule" for military personnel; tasks include reducing soldiers' weight burden and medical evacuation of harmed personnel. Sensitive payloads like an injured soldier, or sensitive electronic or chemical equipment, cannot endure high-energy, high-frequency vibrations above a certain threshold without posing a major safety concern during transit. Such settings present a need for ground vehicles to reduce high-frequency vibrations while traversing unknown terrain, without significantly compromising movement speed.

Since many state-of-the-art robotic platforms — Jackal, Argo J8, and Clearpath J5 - come unequipped with vehicle suspension, we are particularly concerned with achieving high-frequency noise mitigation through a novel controller architecture. Moreover, we wish for our approach to be based on portable commercial off-the-shelf components, so as to ensure the widest possibility of proliferation on existing ground vehicle fleets, without the need of a costly retrofitting campaign. To accomplish this objective, we develop a two-step approach to trajectory planning based on a set of mission-dependent waypoints. Given a desired nominal velocity, as well as a maximum permitted velocity, our approach aims to smoothly vary the vehicle's speed to actively suppress high-frequency vibration normal to the terrain. To this end, we introduce an intuitive vehicle- and terrain-agnostic high-frequency vibration measure which is used to command a desired maximum velocity. The frequency content is measured using a low-cost off-the-shelf inertial measurement unit. We use an optimal feedback controller to minimize incurred cost while converging to the desired waypoint.

2 Prior Work

Previous work on noise and vibration mitigation has chiefly focused on terrain determination based on the pseudo-spectral density of the vibrations, allowing for discrete gain or controller switching [1, 11, 25]. Such approaches only work when the terrain that will be encountered is known a priori, with the classification model depending directly on the vehicle under consideration. Unlike these methods, we provide a means of continuously adapting to changing terrain conditions without the need for pre-classifying the terrain types that may be encountered [14, 19] or the need to introduce additional haptic sensors [4, 8, 15]. In addition, only the tracking controller is dependent on the vehicle properties, with no knowledge assumed about the frequency response properties of the vehicle to vibrations.

Beyond these terrain-classifying approaches, other traditional approaches to vibration mitigation can be divided into two categories: approaches that are concerned with mitigating vibration induced by the vehicle's internal components

Fig. 1. Clearpath Jackal unmanned ground vehicle [4]

(e.g., the engine, transmission, suspension, etc.), and those that deal with external effects (e.g., speed humps, degraded road surfaces, unstructured terrain). We refer to the first category as internal vibrations, and the latter as external vibrations. Internal vibration mitigation has chiefly been centered around damping the resonance response among internal components [23], whereas external vibration mitigation can be further divided into active and passive approach.

Passive external vibration suppression is governed by the fixed suspension design of the vehicle, whereas active suspension systems make use of controlled actuators to complement the passive springs and dampers [27]. In this work, we do not expect the vehicle to have any type of suspension system, thus limiting our control inputs to wheel torque/velocity, steering angle, etc.

We leverage an off-the-shelf inertial measurement unit to obtain a measure of the severity of the vehicle vibrations. In particular, we focus on vibrations that are perpendicular to the vehicle. Frequency properties of the vibrations are obtained by applying a fast Fourier transform (FFT) to a small time window of sampled data. We use frequency content in a precompensated integral controller (PCIC) to obtain the maximum vehicle speed needed to suppress the vehicle's vibrations. This maximum velocity is then applied to the control input - obtained from a tracking linear quadratic requlator (LQR) - by simply scaling the control input to produce an admissible control input. The LQR controller is obtained from a discretized and periodically linearized kinematic model of the vehicle.

We demonstrate the proposed control law on a Clearpath Jackal unmanned ground vehicle (UGV), shown in Figure 1, using only the internal wheel encoders and a low-cost inertial measurement unit as sensor feedback. During the experimental trials, we subject the vehicle to different terrain types (concrete,

[4] Video of the controller applied to the Jackal UGV can be found at https://uofi.box.com/s/9lvx16hrrw7kr4ew7og91w4uspid3n02.

grass, mulch) along a fixed desired path, and we compare the reduction in high-frequency vibrations when using our adaptive speed-based control law compared to a traditional fixed velocity control law.

3 Waypoint Tracking Controller

We first present the kinematic vehicle model used as part of our LQR tracking controller. We then make use of the LQR to generate the system inputs to guide our vehicle to the desired waypoints. Our vehicle hardware limitations restricted our usage of torque-based control and a full dynamics model; rather, we commanded wheel velocities from a derived kinematics model.

3.1 Vehicle Kinematics

The classical equation to represent the dynamics of a nonholonomic mobile robot can be obtained from the Lagrangian formulation [6]:

$$M(q)\ddot{q} + V_m(q,\dot{q})\dot{q} + G_m(q) + \tau_d = B(q)\tau - A^T(q)\lambda, \tag{1}$$

where $q \in \mathbb{R}^n$ is the generalized state, $\tau \in \mathbb{R}^r$ is the input vector, $\lambda \in \mathbb{R}^m$ is the vector of constraint forces, $M(q) \in \mathbb{R}^{n\times n}$ is a symmetric and positive-definite inertia matrix, $V(q,\dot{q}) \in \mathbb{R}$ is the matrix of Coriolis and centrifugal forces, $G(q) \in \mathbb{R}^n$ is the vector of gravitational forces, $\tau_d \in \mathbb{R}^n$ is the vector of disturbances, $B(q) \in \mathbb{R}^{n\times r}$ is the input transformation matrix, and $A(q) \in \mathbb{R}^{m\times n}$ is the matrix associated with any constraints (frictional cone, maximum acceleration, etc).

The above model is widely used in the development of multipurpose controllers, but such controllers generate torque commands, as opposed to velocity commands which are more commonly implemented in commercial robotics. Thus, the use of such a model utilizing torque commands requires additional knowledge of the actuation system of the robot [20], i.e., knowledge regarding the actuator dynamics and model of internal mechanisms relating motor torque to the angular velocity of the wheels. Such information is not readily available for the Jackal UGV. Moreover, the motors on the Jackal have a high gearing reduction which makes torque-based control difficult to implement since the nonlinear friction dynamics, $\eta(t,q,\dot{q})$, become non-negligible at these high gearing ratios:

$$\tau = K_t i + \eta(t,q,\dot{q}).$$

Thus, we will base our controller design on a velocity-based kinematic model of the Jackal where wheel velocity input commands are utilized directly to manipulate system behavior.

We now derive the planar kinematics of an unmanned ground vehicle. In this work, we assume the vehicle maneuvers without slipping, and that the vehicle is based on differential (or skid) steering. Existing skid steering models utilize left and right angular wheel speeds to produce the kinematic and dynamic equations that relate the tire radius and frame size to translational velocities [17]. In

contrast, the Jackal UGV comes equipped with its own skid steer controller that takes into account these parameters for direct control of translational velocity in the x and y directions shown in Figure 2.

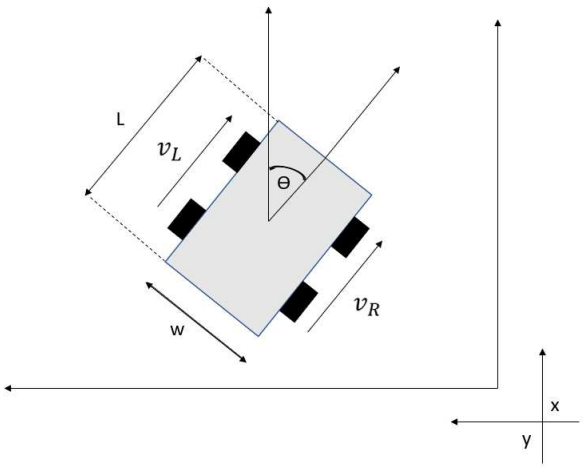

Fig. 2. Kinematic diagram the Jackal unmanned ground vehicle based on differential steering

As a result of the discussion above, most market-available ground robots utilize velocity controllers to track input reference velocities. As such, we developed a velocity controller consistent with the kinematic diagram illustrated in Figure 2 following the approaches of [2, 12]. The resulting kinematics model is as follows:

$$\begin{bmatrix} \dot{x} \\ \dot{y} \\ \dot{\theta} \end{bmatrix} = \begin{bmatrix} \frac{1}{2}(v_L + v_R)\cos\theta \\ \frac{1}{2}(v_L + v_R)\sin\theta \\ (v_R - v_L)/w \end{bmatrix}, \tag{2}$$

such that v_L and v_R are the velocities of the left and right wheels, θ is the heading angle, and $w = 0.4$ m is the vehicle's track width.

The derived model is utilized for direct control of translational velocities and the angular velocity on a two-dimensional plane.

3.2 LQR Tracking Controller Design

We employ a discrete-time linear quadratic regulator (LQR) to navigate towards waypoints by using the current state. We first present vehicle dynamics (2)

linearized about heading angle θ_0:

$$\begin{bmatrix} \dot{x} \\ \dot{y} \\ \dot{\theta} \end{bmatrix}_{\theta_0} = \begin{bmatrix} \frac{1}{2}\cos\theta_0 & \frac{1}{2}\cos\theta_0 \\ \frac{1}{2}\sin\theta_0 & \frac{1}{2}\sin\theta_0 \\ -\frac{1}{w} & \frac{1}{w} \end{bmatrix} \begin{bmatrix} v_L \\ v_R \end{bmatrix}. \tag{3}$$

We proceed by discretizing the above linear system dynamics using an exact zero-order hold discretization approach based on exponential matrices [5, p. 99]. The sampling period that we consider in this work is $\Delta t = 0.01$ s. We now introduce the state and control penalty matrices that we have considered in this work:

$$Q = \operatorname{diag}\left(\left[5, 5, 0.5\right]\right), \quad R = I_{2\times 2}, \tag{4}$$

where Q is the state penalty matrix, and R is the control penalty matrix. These matrices were found in tuning of our simulation and on hardware platform. With this configuration, we prioritize position tracking over heading tracking by more heavily penalizing deviation from the desired positions. For different vehicles, different gain values may be required to obtain control inputs of suitable magnitudes for the actuators. In this work, we have employed a custom finite horizon LQR algorithm of 50 iterations to obtain feedback gain matrix $K \in \mathbb{R}^{2\times 3}$. We relinearize the model and recompute this gain every five seconds.

We implement the controller as follows:

$$\vec{u} = K(\vec{x}_{\text{des}} - \vec{x}),$$

where $\vec{x} \in \mathbb{R}^3$ denotes the full vehicle state, $\vec{x}_{\text{des}} \in \mathbb{R}^3$ corresponds to the current desired waypoint, and $\vec{u} \in \mathbb{R}^2$ corresponds to the desired right and left wheel velocity.

4 High-Frequency Vibration Compensator

As mentioned in the introduction, we wish to regulate the speed of the vehicle to control the severity of high-frequency vibrations. This task naturally poses the question of what constitutes a usable measure of the high-frequency vibration content. We discuss such a measure at the beginning of this section. Given this measure, we then design a compensator to adjust our maximum desired speed.

Given a measure of the high-frequency content, we may then design a model-free controller that outputs a speed limit, which is consequently applied to the control input obtained from the LQR controller in Sec. 3.2.

4.1 High-Frequency Vibration Measure

As mentioned previously, we will draw on linear acceleration readings of a low-cost off-the-shelf inertial measurement unit (IMU) to obtain the strength of high-frequency vibrations. Here, we discuss two candidate measures for the high-frequency content, of which the latter will ultimately be used.

We start with a sampled data signal of the linear acceleration measures. We assume that the IMU is mounted on the vehicle such that the internal z-axis faces normal to the level plane of the vehicle. We first consider the case of a single acceleration signal, expanding to the case of multiple signals afterwards.

Let $a(t)$ be the acceleration signal that we wish to be limited in its high-frequency power. Since we will consider the signal properties in the frequency domain, we will have to obtain sampled time windows of this continuous-time signal, on which we apply a discrete Fourier transform.

Let $a(t)$ be sampled at sampling frequency f_s. We wish to obtain sampled windows of $a(t)$ of duration Δt_{win}, such that each window contains $N_{\text{win}} = f_s \Delta t_{\text{win}} \in \mathbb{N}$ samples. We denote each window by $a_k = \{a(k\Delta t_{\text{win}}), a(k\Delta t_{\text{win}} + 1/f_s), a(k\Delta t_{\text{win}} + 2/f_s), \ldots, a((k+1)\Delta t_{\text{win}})\}$, where $k \in \mathbb{N}$. We may then apply a discrete Fourier transform (DFT) [24], [26] on each of these windows, such that we obtain $\alpha_k[f]$, where $f \in F := \{0, f_s/(2(N_{\text{win}} - 1)), 2f_s/(2(N_{\text{win}} - 1)), \ldots, f_s/2\}$. The latter maximum frequency $f_s/2$ is the Nyquist frequency. The value of $\alpha_k[f]$ denotes the power of the signal for frequencies in the range $[f, f + f_s/(2(N_{\text{win}} - 1))]$.

Multiple acceleration signals. Let us now consider the case where we have multiple accelerations that we could like to consider. We denote these n accelerations by $a^{(1)}, \ldots, a^{(n)}$. One approach to combining these signals is by taking a linear combination to obtain

$$a = \sum_{i=1}^{n} b_i a^{(i)},$$

such that $\sum_{i=1}^{n} b_i = 1$ and each $b_i > 0$. This does, however, not preclude the possibility of destructive interference between the various signals, which may make for a signal power of a that is less than that of one of its constituent signals $a^{(i)}$. One could elect to consider $|a^{(i)}|$ instead, but this would not account for the effect of high-frequency sign changes in each signal, which would skew the DFT towards lower frequencies.

A more reasonable approach would be to consider DFT results of the acceleration signal $\alpha_k^{(i)}$, and treat each result as a vector in $\mathbb{R}^{N_{\text{win}}}$. Since each element in each $\alpha_k^{(i)}$ is nonnegative, we can now consider

$$\alpha_k = \sum_{i=1}^{n} \beta_i \alpha_k^{(i)},$$

with the stipulation that $\sum_{i=1}^{n} \beta_i = 1$ and each $\beta_i > 0$. The addition of signal powers is clearly constructive, and allows us to place greater emphasis on some signals by increasing the magnitude of the pertinent β_i coefficients.

Implications of sampling parameter choice. Having obtained the discrete Fourier transform of the acceleration signal for window k, we now make a number

of observations on the importance of the sampling rate f_s and window duration Δt_{win}. It is clear from the Nyquist frequency that a higher sampling rate is directly related to a higher observed maximum frequency. In practice, terrain induced vibrations encountered during trials rarely affect frequencies above 20 to 30 Hz.

With regards to the effect of the window duration, a longer duration allows one to capture more samples, thus allowing for greater resolution in the DFT results. In addition, low frequency values are now distributed much more finely, compared to when Δt_{win} is small. In the case of small Δt_{win}, $\alpha_k[0]$ often accounts for most of the signal's energy, thereby providing less fine-grained control over period high-frequency vibrations.

On the other hand, a longer window duration implies that there is a greater time lag between the DFT results and the time when the terrain features that produced such a frequency response were present. Since control-based on signal frequency content will always be reactive, this feature results in a trade-off between lower frequency resolutions and greater time-delay in producing adequate responses to rapidly changing terrain. In this case, a sliding or moving window approach will not correct for this time lag, since the values obtained in this way will only relate to a process that started time Δt_{win} ago. In addition, an increased window duration will also "blend" new terrain responses with old ones, which would result in a skewed representation of the near-term external vibrations experienced.

4.2 High-frequency content measure.

We can now proceed to define a measure of the high-frequency content. We first define a *threshold frequency* $f_{\text{th}} < f_s/2$, which marks the transition from low to high frequencies. Since we wish to encode the effect of all high frequencies, it would be natural to take the integral of the Fourier transform to account for the power of all high frequencies. Since we are working with discrete values, we instead consider a weighted sum of the following form:

$$r_{k,\text{hf}} = \frac{f_s}{2(N_{\text{win}} - 1)} \sum_{f \in F : f \geq f_{\text{fs}}} \alpha_k[f].$$

It should be noted that the magnitude of $r_{k,\text{hf}}$ is directly dependent on the magnitude of the underlying signal $a(t)$. Thus, for a terrain with high amplitude, lower frequency vibrations, a high value of $r_{k,\text{hf}}$ may be obtained, whereas for a terrain with high-frequency vibrations of lower amplitude, a low value of $r_{k,\text{hf}}$ is obtained. This feature makes for a very cumbersome controller design, where one would need to schedule gains based on the signal strength or prior knowledge of the terrain that is to be traversed. Moreover, a controller that is tuned for one vehicle would not be transferable to a different vehicle, since the signal power may be higher or lower. This serves as an alternate solution to the method proposed in this paper.

To avoid these problems, we define the following measure:

$$r_k = \frac{f_s}{2(N_{\text{win}} - 1)} \frac{\sum_{f \in F: f \geq f_{\text{fs}}} \alpha_k[f]}{\sum_{f \in F} \alpha_k[f]}. \tag{5}$$

where k represents the time-step unit. This ratio is agnostic of the signal power, and is much more intuitive to reason about. One would be able to say that 10% of the signal power is permitted to be of a high-frequency, regardless of the vehicle properties. For this reason, we will use this nondimensional measure in our controller design, which we refer to as the *high-frequency content ratio*.

4.3 Velocity Regulator Design

Having defined a measure for the high-frequency external vibrations, we can now proceed to design a model-free velocity regulator that aims to regulate this quantity around a predefined setpoint.

Since the terrain is not known a priori, this controller will be, out of necessity, reactive. We have chosen to design an integral controller with precompensation (PCIC), as described next.

We would like to start out with a nonzero allowable speed defined by the mission, a nominal speed $V_0 > 0$. V_0 serves as the speed the vehicle would like to travel along all terrains given minimal vibrations. In this work, given the limitations of the Jackal UGV, this speed is taken to be 1 m/s in consideration of our UGV's capabilities. We would like to regulate the maximum allowable speed on the different terrains. Applying this controller to more sophisticated robots that can operate at faster speeds is left for future work.

As mentioned previously, a decrease in the vehicle's speed is related to a decrease in the high-frequency vibration content. For this reason, it is most intuitive to decrease the vehicle's maximum permissible speed when the high-frequency vibrations exceed the user-defined threshold, and increase the speed if r_k is too low. We define the high-frequency content ratio set point as $r_0 > 0$. In practice, r_0 will have to be sufficiently large so as to overcome ambient noise in the IMU. Moreover, a larger r_0 allows the vehicle to traverse bumpier terrain at faster velocities. This trade-off must be kept in mind while choosing this constant. In the following, we refer to r as the value r_k that corresponds to the most recent sampling window.

We have elected to regulate r by means of an integral controller that acts on the error $e = r_0 - r$. This choice of controller design, over a proportional controller, stems from a desire to prevent control-induced high-frequency vibrations. In a proportional controller, instantaneous changes are immediately acted upon, forcing jump changes in the maximum speed. In practice, this induces abrupt, undesirable braking action and acceleration.

An integral controller also faces a number of challenges. When the vehicle is stationary, the integral controller will continue accumulating as noise from the IMU is integrated. This in turn leads to the issue of integral windup. We overcome this issue by introducing an integral with projection. The accumulated

integration from the current time step is given by I_i and the saturated value, I_o, is given as follows:

$$I_o = \text{proj}_{[-V_0, V_{\text{lim}} - V_0]}(I_i + K_i e \Delta t_{\text{win}}). \tag{6}$$

In (6), $K_i > 0$ scales the output error fed into the integration. A higher gain implies a more aggressive response in the change of the maximum permissible speed. K_i is to be limited in practice when rough terrain is expected during a mission, since controller-induced vibrations are aggravated in such settings.

In (6) we also introduce a projection (or, in this case, 'clamping') operator. The limits of the projection operator are $[-V_0, V_{\text{lim}} - V_0]$, where V_{lim} is the user-defined limiting speed of the vehicle, such that $V_{\text{lim}} \geq V_0$. The significance of this result will become apparent below.

We obtain the maximum speed from this controller by taking $V_{\text{max}} = I_o + V_0$ at each time step. We proceed by showing how this maximum speed is applied to the control command given by the LQR controller of Sec. 3.2.

Vehicle speed regulation. Given a control command $\vec{u}$, we can compute the vehicle's speed by means of (3). We define the commanded vehicle speed as $V_{\text{cmd}} = \sqrt{\dot{x}^2 + \dot{y}^2}$. We identify two cases: the case where $V_{\text{cmd}} \leq V_{\text{max}}$, and the case where $V_{\text{cmd}} > V_{\text{max}}$.

In the former case ($V_{\text{cmd}} \leq V_{\text{max}}$), we apply $\vec{u}$ to the vehicle. This case will most often arise when we are close to our waypoint $\vec{x}_{\text{des}}$ as the error in the desired position fed into LQR controller will be much smaller. In the latter case ($V_{\text{cmd}} > V_{\text{max}}$), we have chosen to scale the velocity command as follows:

$$\vec{u}_{\text{cmd}} = \frac{V_{\text{max}}}{V_{\text{cmd}}} \vec{u}. \tag{7}$$

It is obvious that this scaling results in a commanded velocity of magnitude V_{max}, as is desired.

This form of speed regulation raises the question of waypoint convergence, as the vehicle's velocity may converge to zero before it converges to the waypoint since our error will be small close to the waypoint. In practice, given that r_0 is taken to be greater than the value encountered at ambient noise, and given a sufficiently large limit speed V_{lim}, as well as a sufficiently large gain K_i, the vehicle will converge to the waypoint on all terrains encountered in practice.

The complete controller architecture is given in Fig 3. We will refer to this architecture as an *LQR-I controller*, short for combined LQR and precompensated integral controller.

Considerations in tuning. We now discuss a number of practical considerations in tuning the proposed controller. The presented algorithm contains the following tuning parameters:

– State and control penalty matrices Q, R;

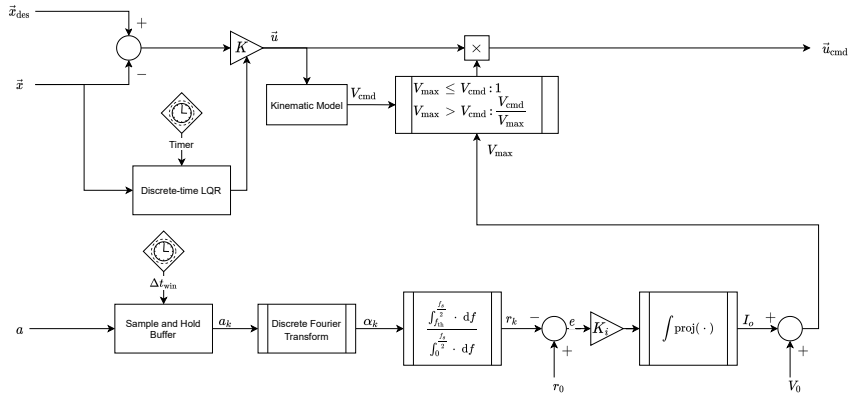

Fig. 3. Block diagram of the combined LQR and precompensated integral controller.

- Nominal and limit velocity V_0, V_{lim};
- High-frequency content ratio setpoint r_0, threshold frequency f_{th}, and integral gain K_i;
- Sampling frequency f_s and window duration Δt_{win}.

The state and control penalty matrices of the LQR controller can be designed beforehand on nominal terrain types. The projection operator of (6) ensures that the vehicle speed will not exceed V_{lim}. In this work, $V_{\text{lim}} = 2$ m/s. As mentioned before, V_0 can be assumed to be a mission defined parameter, loosely related to the nominal mission speed, although it could be overruled in the case of sufficiently harsh terrains.

The high-frequency content ratio setpoint r_0 can be tuned heuristically by accounting for ambient sensor noise. In the authors' experience, the most straightforward way is to slightly vary it until the vehicle's perceived motion is sufficiently smooth. The same advice extends to the threshold frequency (f_{th}), although in our experience a value of 5 Hz worked for all trials. When taking too high of a value, it is often the case that only sensor noise is accounted for. This phenomenon may be aggravated by a poor choice of Δt_{win}, since a low duration tends to lump most of the signal power in the lowest frequency buckets. Conversely, too high of a window duration causes intolerable time delays in registering the lag of the control signal, as mentioned previously.

The integral gain K_i, as mentioned previously, dictates how aggressively the controller reacts to vibration changes. It is key to properly tune this value, since controller-induced vibrations may quickly arise if this value is too high. In fact, a sufficiently large value of K_i can cause repeated start/stop action at a frequency of $1/(2\Delta t_{\text{win}})$.

Finally, f_s should at least be twice the desired maximum frequency. This could mean that frequencies as low as 20 Hz could potentially yield satisfactory performance. Window duration Δt_{win} has been found to yield the best results when taken to be 1 s.

These parameters may require tuning as per user-defined goals and mission objectives. It is important to note that although we developed a controller to operate on the Jackal vehicle, the same control structure could be implemented on other UGVs. Demonstration of this application is reserved for future work.

5 Experiments & Results

We implemented the novel controller on the Jackal UGV performing in various terrains and collected the high-frequency noise and velocity content data. We compared our controller to an open-loop test case to assess performance. We compare high-frequency noise content and velocity command following for paved concrete, grass, and mulch surfaces. Data is collected for transitions between surfaces to illustrate the robustness of the implemented control algorithm and show improved performance over all tested terrain.

For all trials, given the maximum speed of the Jackal is $V_{\text{lim}} = 2$ m/s; we run the Jackal with a nominal speed $V_0 = 1$ m/s. For the following experiments, the vehicle is subjugated to identical terrain. The vehicle first moves through with an open-loop controller with a fixed reference velocity without consideration of the high-frequency content. Second, a closed-loop test is performed with the proposed controller where the maximum permissible velocity is modified in real time to mitigate vibrations impacts. The results form both test runs are compared.

Obviously, performance is altered by the choice of integrator gain. A large gain compensation results in faster changes to calculated V_{max}, which results in more oscillatory behavior. Through experimental trials, a good range of integrator gains was found to be $K_i \in [2, 4]$. The gain parameters were tuned before the experiments for optimal results, however, in practice this tuning is unnecessary since the controller exhibits improved performance over all tested surfaces while $K_i \in [2, 4]$. We set the high-frequency threshold for all experiments to be 5 Hz, while the remaining parameters f_s, Δt_{win}, Q, and R are equal to the values defined in previous sections.

The controller was implemented onboard the vehicle in Python 2.7 on an NVidia Jetson TX2 computer running Ubuntu 16.04 and ROS Kinetic. Low-level controller commands were passed through the appropriate ROS topics provided by Clearpath. The IMU used was a WaveShare 10 DOF IMU sensor board, which was interfaced with the UGV through an Arduino Mega 2560. The controller published input updates at 100 Hz, while IMU updates were read at 60 Hz.

5.1 Concrete Performance

Like many unmanned ground vehicles, the Jackal is designed with multipurpose maneuverable capabilities. One commonly encountered surface is concrete, and thus to illustrate the capabilities of the LQR-I controller, we first analyze its performance on a tiled concrete terrain. Figures 4 and 5 display the Jackal's performance autonomously navigating over concrete surfaces with open-loop control (fixed movement speed of V_0), and the closed-loop LQR-I controller, respectively.

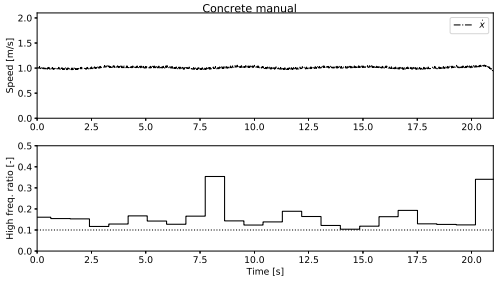

Fig. 4. Open-loop control with nominal velocity $V_0 = 1$ meter per second.

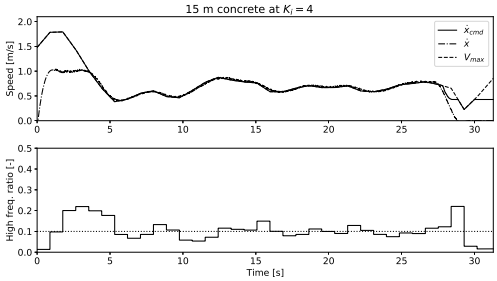

Fig. 5. Closed-loop LQR-I control with nominal velocity $V_0 = 1$ compensating high-frequency vibration content output such that r_k tracks $r_0 = 0.1$. Measured heading speed $\dot{x}$ is closely compared to the heading command $\dot{x}$ and maximum velocity V_{max} set by the controller.

The open-loop manual control results in a steady velocity output that follows the nominal input speed command regardless of high-frequency noise. Given the generally smooth surface of concrete, the high-frequency noise content stays largely steady with the exception of some oscillations created by divots in the path when transitioning from one concrete tile to another. Despite the smooth surface and terrain, the high-frequency noise content ratio in Figure 4 is consistently above the set threshold $r_0 = 0.1$.

Figure 5 illustrates the enhanced performance of the Jackal as controlled by the proposed LQR-I controller with a tuned integral gain $K_i = 4$. As the vehicle begins moving, a large change in initial speed causes unwanted vibrations. Yet, within approximately 5 seconds, the controller is able to compensate for the unwanted initial high-frequency noise, decreasing the ratio to below the setpoint. As explained in the previous section, as r_k decreases below the set threshold, the LQR controller increases control action with input $\vec{u}$ as $V_{\text{cmd}} \leq V_{\text{max}}$. This causes the high-frequency ratio to increase until it exceeds its given threshold, at which point the integrator compensates by decreasing the control action to $\vec{u}_{\text{cmd}}$ as outlined in equation (7).

Note that the controller exhibits both impressive velocity tracking and high-frequency noise tracking. That is, not only is the high-frequency noise generally kept at the desired threshold, the heading speed also closely follows the heading command and maximum velocity set by the controller. This is largely due to the robust properties of the LQR and integral controllers tasked with producing optimal input commands, i.e., the LQR-I controller exhibits low peak sensitivities at high frequencies [13, 16], and good low frequency command following with high complementary sensitivities at low frequencies. With proper tuning, as the high-frequency noise ratio increases, the integral controller attenuates high-frequency noise with guaranteed convergence with added saturation limits, and as high-frequency noise drops below the predefined threshold, LQR increases the velocity to closely follow the nominal speed V_0. To further test controller performance, we implement the LQR-I controller on grass, where larger vibrations produce more high-frequency noise content.

5.2 Grass Performance

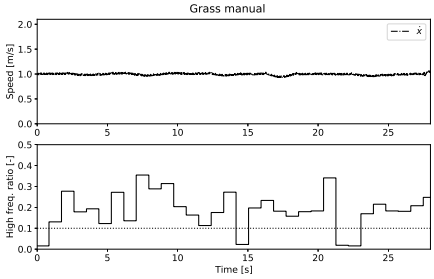

Fig. 6. Open-loop control with nominal velocity $V_0 = 1$ meter per second.

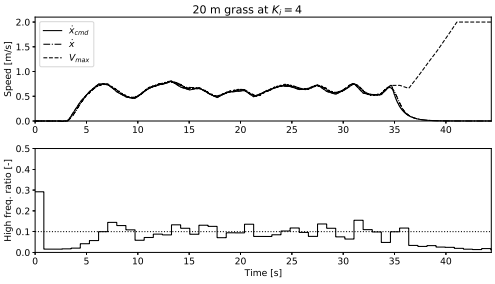

Fig. 7. Closed-loop LQR-I control with nominal velocity $V_0 = 1$ compensating high-frequency vibration content output such that r_k tracks $r_0 = 0.1$.[6]

To further illustrate the performance and robustness of the proposed control architecture, the Jackal travels on rougher terrains such as grass, where we expect to see significantly larger high-frequency noise [18]. By inspection, one can easily note from Figure 6 that the open-loop control of the Jackal exhibits a substantially larger amplitude for the high-frequency noise ratio r_k traversing grass in comparison to maneuvering on concrete. Similar to the previous example, the open-loop controller accurately follows the nominal speed of $V_0 = 1$ meter per second.

This example further highlights the controller performance and ability to reduce unwanted high-frequency noise content while riding the boundary of the maximum permissible vehicle speed. Consistent with previous results, the high-frequency ratio has accurately been reduced to lightly oscillate about $r = 0.1$. At the same time, the heading speed $\dot{x}$ is nearly identical to the controller heading command $\dot{x}_{\text{cmd}}$ given by the LQR-I controller and the maximum velocity $V_{\max}$ determined by the speed regulator. The only substantial deviation happened as the Jackal slowed to a stop while nearing its waypoint, causing the high-frequency noise content to diminish to 0, which in turn set $V_{\max} = 2$ meters per second.

Figures 5 and 7 display a vast improvement in Jackal's performance when compared to the open-loop controller in closely following a set high-frequency noise content ratio while riding the boundary of the optimal permissible velocity. Given the data shows the controller capabilities on smooth and difficult terrain, we now aim to show improved controller performance when changing from one environment to another.

5.3 Multi-terrain Performance

The final set of experiments contain data consisting of the speed and high-frequency noise ratio as a function of time as the Jackal traverses concrete and mulch over a distance of 15 meters. A vertical, red dotted line in Figures 8 and 9 denotes the distance at which the UGV transitions from concrete to mulch. One can observe from Figure 8 that the amplitude of the high-frequency ratio is significantly larger when maneuvering on mulch than concrete.

It is important to note that although the open-loop controller follows the nominal velocity closely, there exists no point in time where the high-frequency content is below the set threshold. Conversely, the closed-loop LQR-I controller exhibits the ability to compensate performance to keep r_k near the assigned threshold regardless of changes in terrain while accurately tracking desired heading and maximum velocity commands. Thus, Figure 9 empirically shows a promising example of the controller being capable of travelling multiple unknown surfaces without a priori knowledge regarding the environment.

In comparison to the previous two examples, the average speed in Figure 9 is slower, i.e., the controller produces an output velocity that is further from

[6] Video of the controller applied to the Jackal UGV can be found at https://uofi.box.com/s/9lvx16hrrw7kr4ew7og91w4uspid3n02.

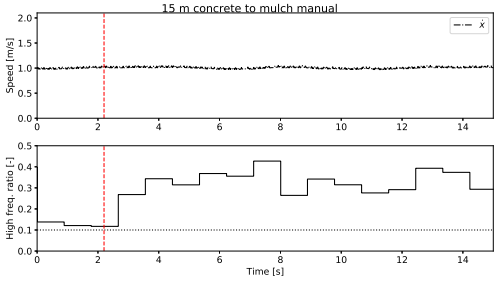

Fig. 8. Open-loop control with nominal velocity $V_0 = 1$ meter per second.

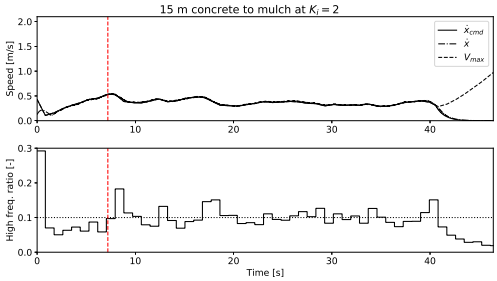

Fig. 9. Closed-loop LQR-I control with nominal velocity $V_0 = 1$ compensating high-frequency vibration content output such that r_k tracks $r_0 = 0.1$

the nominal value $V_0 = 1$. This phenomenon is a result of the following factors: (i) mulch being a particularly uneven surface that causes large high-frequency amplitudes [18] and (ii) the integrator gain $K_i = 2$ being lower than its value in the previous two examples, where $K_i = 4$, which encourages speed maintenance. Since mulch is an unpredictable, uneven surface, the gain K_i is tuned lower to help diminish controller-induced vibrations. In general, a lower K_i gain is advisable when particularly unstructured terrain is expected, although as stated previously, it is not necessary to tune the gain differently depending on the terrain for improved performance.

These three examples illustrate that the proposed controller results in improved UGV performance to mitigate undesirable high-frequency noise regardless of the terrain. Out of all tuning parameters, adopting a lower K_i value appears to be key in handling unstructured terrain, whereas the LQR and frequency threshold settings can remain fixed regardless of the specifics of the current mission.

6 Conclusion and Future Work

This paper presents a controller architecture to attenuate unwanted high-frequency vibrations during transit of a ground vehicle, while preserving waypoint tracking capabilities at reasonable speeds. The control system provides a method of maneuvering on unknown terrain while limiting damage to sensitive payloads due to high-frequency vibrations. In a sense, this controller mimics a natural human-like response while driving over various terrains - as the roughness of the terrain changes humans adjust the speed of the vehicle to minimize sudden impulses and prevent damage to the passengers and cargo inside. Furthermore, this speed modulation can be achieved without the need of perception, terrain identification, or extensive training.

Experiments indicate that regardless of noise introduced by unknown obstacles over variable terrain, the proposed control architecture is capable following a desired trajectory at the maximum velocity governed by the experienced vibrations and high-frequency noise. We implemented the controller on a vehicle over concrete, grass, and mulch. Regardless of the high-frequency vibration content, the vehicle was able to perform its primary objective of moving to a desired waypoint at the maximum permissible velocity while staying below the high-frequency content ratio threshold.

In this work, the novel control system has been implemented on the Clearpath Jackal UGV, a vehicle with a maximum speed of 2 m/s. This same control structure can be scaled to larger systems with more capability without requiring much retuning, eventually being implemented in scenarios for medical evacuation and carrying various sensitive payloads. As the controller is implemented on more complex systems, controller capabilities can consequently be enhanced. With a higher maximum velocity, a proportional integral derivative controller can be utilized for faster convergence to the desired waypoint, with added saturation or a pre-filter to account for unwanted overshoot, and a low-pass filter to prevent controller-induced vibrations.

Future work includes the use of a high-fidelity dynamic vehicle model to loosen assumptions on non-slipping movement, which often does not hold on highly unstructured terrain. This generalization would further be supported by a transition to direct torque control, allowing for additional adaptive control capabilities. In addition, model-based filtering techniques may be used to filter out low frequency components of the accelerations, thereby only considering terrain-induced random noise. Finally, terrain classification may be possible using the proposed high-frequency content ratio, as well as new measures based on other sensors, such as piezo-electric haptic feedback and LIDAR sensing.

References

1. Brooks, C., Iagnemma, K., Dubowsky, S.: Vibration-based terrain analysis for mobile robots. In: IEEE International Conference on Robotics and Automation. pp. 3415–3420. IEEE (2005)

2. De La Cruz, C., Carelli, R.: Dynamic model based formation control and obstacle avoidance of multi-robot systems. Robotica **26**(3), 345–356 (2008)
3. Debenedictis, T.A., Fraysse, F., Milanese, S., Tomkinson, G., Billing, D., Furnell, A., Thewlis, D.: The simulation of the whole-body vibration experienced during military land transit. Human Factors and Mechanical Engineering for Defense and Safety **2**(1) (2018)
4. Filitchkin, P., Byl, K.: Feature-based terrain classification for littledog. In: IEEE/RSJ International Conference on Intelligent Robots and Systems. pp. 1387–1392 (2012)
5. Franklin, G.F., Powell, J.D., Workman, D.L.: Digital control of dynamic systems. Addison-Wesley, 3 edn. (2002)
6. Fukao, T., Nakagawa, H., Adachi, N.: Adaptive tracking control of a nonholonomic mobile robot. IEEE transactions on Robotics and Automation **16**(5), 609–615 (2000)
7. Grzesica, D.: Measurement and analysis of truck vibrations during off-road transportation. MATEC Web of Conferences **211**, 13003 – 13008 (2018)
8. Hoepflinger, M.A., Remy, C.D., Hutter, M., Spinello, L., Siegwart, R.: Haptic terrain classification for legged robots. In: IEEE International Conference on Robotics and Automation. pp. 2828–2833. IEEE (2010)
9. Khurana, A., Nagla, K.S.: Signal averaging for noise reduction in mobile robot 3D measurement system. MAPAN **33**(1), 33–41 (2018)
10. Lu, F., Ishikawa, Y., Shiina, T., Satake, T.: Analysis of shock and vibration in truck transport in Japan. Packaging Technology and Science **21**(8), 479–489 (2008)
11. Lv, W., Kang, Y., Zheng, W.X., Wu, Y., Li, Z.: Feature-temporal semi-supervised extreme learning machine for robotic terrain classification. IEEE Transactions on Circuits and Systems II: Express Briefs **67**(12), 3567–3571 (2020)
12. Lynch, K.M., Park, F.C.: Modern robotics. Cambridge University Press (2017)
13. Masti, D., Zanon, M., Bemporad, A.: Tuning lqr controllers: a sensitivity-based approach. IEEE Control Systems Letters (2021)
14. Ono, M., Fuchs, T.J., Steffy, A., Maimone, M., Yen, J.: Risk-aware planetary rover operation: Autonomous terrain classification and path planning. In: IEEE Aerospace Conference. pp. 1–10 (2015)
15. Otsu, K., Ono, M., Fuchs, T.J., Baldwin, I., Kubota, T.: Autonomous terrain classification with co-and self-training approach. IEEE Robotics and Automation Letters **1**(2), 814–819 (2016)
16. Prakash, A., Parida, S.: Lqr based pi controller for load frequency control with distributed generations. In: 2020 21st National Power Systems Conference (NPSC). pp. 1–5. IEEE (2020)
17. Rogers-Marcovitz, F.: On-line mobile robotic dynamic modeling using integrated perturbative dynamics. Tech. rep., Robotics Institute at Carnegie-Mellon University (2010)
18. Rosenfeld, R.D., Restrepo, M.G., Gerard, W.H., Bruce, W.E., Branch, A.A., Lewin, G.C., Bezzo, N.: Unsupervised surface classification to enhance the control performance of a UGV. In: Systems and Information Engineering Design Symposium (SIEDS). pp. 225–230 (2018)
19. Rothrock, B., Kennedy, R., Cunningham, C., Papon, J., Heverly, M., Ono, M.: SPOC: Deep learning-based terrain classification for mars rover missions. In: AIAA SPACE 2016. American Institute of Aeronautics and Astronautics (2016)
20. Sim, O., Jung, T., Lee, K.K., Oh, J., Oh, J.H.: Position/torque hybrid control of a rigid, high-gear ratio quadruped robot. Advanced Robotics **32**(18), 969–983 (2018)

21. Streijger, F., Lee, J.H., Manouchehri, N., Melnyk, A.D., Chak, J., Tigchelaar, S., So, K., Okon, E.B., Jiang, S., Kinsler, R., Barazanji, K., Cripton, P.A., Kwon, B.K.: Responses of the acutely injured spinal cord to vibration that simulates transport in helicopters or mine-resistant ambush-protected vehicles. Journal of Neurotrauma **33**(24), 2217–2226 (2016)
22. Vlkovský, M., Veselík, P., Grzesica, D.: Cargo securing and its economic consequences. In: 22nd International Scientific Conference. pp. 129–135. Transport Means, Kaunas University of Technology, Kaunas (2018)
23. Wang, Q., Rajashekara, K., Jia, Y., Sun, J.: A real-time vibration suppression strategy in electric vehicles. IEEE Transactions on Vehicular Technology **66**(9), 7722–7729 (2017)
24. Wang, Z.: Fast algorithms for the discrete w transform and for the discrete fourier transform. IEEE Transactions on Acoustics, Speech, and Signal Processing **32**(4), 803–816 (1984)
25. Weiss, C., Frohlich, H., Zell, A.: Vibration-based terrain classification using support vector machines. In: IEEE/RSJ International Conference on Intelligent Robots and Systems. pp. 4429–4434. IEEE (2006)
26. Winograd, S.: On computing the discrete fourier transform. Mathematics of computation **32**(141), 175–199 (1978)
27. Yuvapriya, T., Lakshmi, P., Rajendiran, S.: Vibration suppression in full car active suspension system using fractional order sliding mode controller. Journal of the Brazilian Society of Mechanical Sciences and Engineering **40**(4) (2018)